

Lightweight Image Super-Resolution with Hierarchical and Differentiable Neural Architecture Search

Han Huang¹, Li Shen^{2*}, Chaoyang He³, Weisheng Dong¹, Haozhi Huang⁴, Guangming Shi¹

¹Xidian University, Xi'an, China, ²JD Explore Academy, Beijing, China

³University of Southern California, Los Angeles, USA, ⁴Xverse, Shenzhen, China

{hanhuang8264, mathshenli}@gmail.com, chaoyang.he@usc.edu,

wsdong@mail.xidian.edu.cn, hertzhuang@xverse.cn, gmshi@xidian.edu.cn

Abstract

Single Image Super-Resolution (SISR) tasks have achieved significant performance with deep neural networks. However, the large number of parameters in CNN-based methods for SISR tasks require heavy computations. Although several efficient SISR models have been recently proposed, most are handcrafted and thus lack flexibility. In this work, we propose a novel differentiable Neural Architecture Search (NAS) approach on both the cell-level and network-level to search for lightweight SISR models. Specifically, the cell-level search space is designed based on an information distillation mechanism, focusing on the combinations of lightweight operations and aiming to build a more lightweight and accurate SR structure. The network-level search space is designed to consider the feature connections among the cells and aims to find which information flow benefits the cell most to boost the performance. Unlike the existing Reinforcement Learning (RL) or Evolutionary Algorithm (EA) based NAS methods for SISR tasks, our search pipeline is fully differentiable, and the lightweight SISR models can be efficiently searched on both the cell-level and network-level jointly on a single GPU. Experiments show that our methods can achieve state-of-the-art performance on the benchmark datasets in terms of PSNR, SSIM, and model complexity with merely 68G Multi-Adds for $\times 2$ and 18G Multi-Adds for $\times 4$ SR tasks. Code will be available at <https://github.com/DawnHH/DLSR-PyTorch>.

1. Introduction

Image super-resolution (SR) is a low-level vision problem that reconstructs a single low-resolution (LR) image to a high-resolution (HR) image. This problem is ill-posed

since multiple HR images can degrade to the same LR image. Many deep-learning-based methods have been proposed to address this problem [6, 15, 20, 18, 45, 46, 8, 25, 23] and have achieved great success.

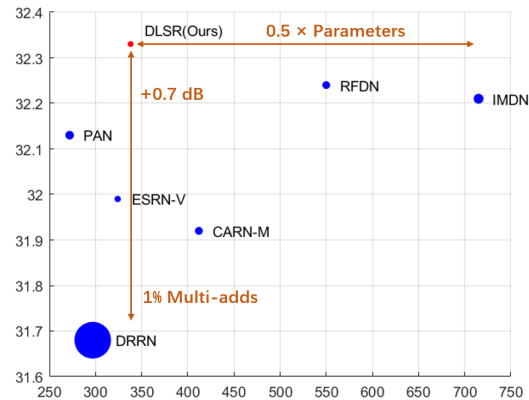


Figure 1. Performance comparison of existing lightweight methods on Set5 [3] ($4\times$). The size of the dot denotes the Multi-Adds of the method. Our method achieve state-of-the-art performance with fewer parameters or fewer Multi-Adds.

While the SR performance is boosted by the deep learning approach, the model complexity is also increased. For example, RDN [46] had 22M parameters and EDSR [20] reached up to 43M parameters. It is difficult to deploy these models to the equipment with low computing power. For real-world applications, lightweight and efficient SR models have also been designed in recent years, including handcrafted SR neural networks [16, 16, 2] and neural architecture search (NAS) based SR methods [5, 32, 19, 27].

Although great improvements have been achieved by existing lightweight SR methods, they still suffer from several limitations. First, hand-crafted lightweight SR models like IMDN [13] and RFDN [22] adopted several 3×3 convolution layers with large amount of parameters and Multi-

*Li Shen is the corresponding author.

Adds. The building blocks designed by these methods with the same three 3×3 convolution layers can also be sub-optimal and lack flexibility for SISR tasks. Second, the network-level architecture of these methods only considered concatenating the output features of the blocks at the end of the model while omitting intermediate information flows among the blocks, which have been demonstrated to enlarge the reception field [11] and could be useful for improving SR performance [36, 29, 46, 30]. However, the network cannot be connected too densely in order to achieve an efficient lightweight SR model. Therefore, it’s important to find which connection benefits the cell most to improve the performance of lightweight SR models while keeping a slightly low model complexity. Finally, Most Neural Architecture Search (NAS) based methods for SR tasks were based on reinforcement learning and evolutionary methods which are time-consuming and require a large number of computing resources to search for appropriate models. Furthermore, they failed to achieve better peak signal-to-noise ratio (PSNR) or structural similarity index measure (SSIM) [38] results with searched lightweight SR models comparing with the existing state-of-the-art (SOTA) hand-crafted SR models.

To address these problems, we propose a lightweight image super-resolution method with a fully differentiable neural architecture search (DLSR) which is composed of cell-level and network-level search techniques. For cell-level search, we design a large search space (see Table 3.1) that contains more lightweight convolution operations to increase the probabilities of finding more lightweight models. As opposed to existing work [21, 32] that searched for arbitrary combinations and connections of basic operations or searched for handcrafted blocks, we search for the operation combinations based on information distillation structure that provides prior knowledge of nice lightweight SR structures. Based on the flexibility of lightweight operation combinations, our search space not only contains the hand-crafted RFDB [22] structure but also explores for a better cell for efficient SR. To utilize the intermediate information flow between the cells, we design a network-level search space that contains all possible connections among the cells to further boost the performance. As opposed to FALSr [5] which uses an evolutionary algorithm to search for block connections with discrete encoding, we first densely connect the blocks to build a super-net, then utilize the continuous relaxed architecture parameters to weigh the connections and optimize the parameters with the stochastic gradient descent method. During searching, the network automatically identifies the most important intermediate information flow connections.

In addition, we design a loss function composed of three parts: L1 loss, High Frequency Error Norm (HFEN) loss [28], and the number of parameters of the operations.

HFEN is an image comparison metric from medical imaging and uses a Laplacian of Gaussian kernel for edge-detection. Thus, the HFEN loss can help to minimize the reconstruction error of high-frequency image details. In addition, we treat the number of parameters of the operations as a regularization term to push the searching direction into a more lightweight space. Experimental results show that our DLSR method surpasses other SOTA lightweight SR methods in terms of PSNR, SSIM with fewer parameters and Multi-Adds on benchmark datasets: Set5 [3], Set14 [39], B100 [26], and Urban100 [12] in $\times 2, \times 3, \times 4$ super-resolution tasks. In the end, our main contributions are summarized as three-fold:

- We propose a differentiable NAS strategy for searching a lightweight SR model, which incorporates both cell-level and network-level search spaces to strengthen the SR performance. The proposed approach significantly reduces the searching cost compared to existing RL-based NAS methods.
- We design a loss function that considers distortion, high-frequency reconstruction, and lightweight regularization that push the searching direction to explore a better lightweight SR model.
- We conduct extensive experiments to evaluate the efficacy of our method, which achieves state-of-the-art performance on the benchmark datasets in terms of PSNR, SSIM, and model complexity.

2. Related work

2.1. CNN-based Image Super-Resolution

SR performance has been greatly improved by CNN-based methods [6, 15, 34, 20, 18, 45, 46, 37, 44, 43, 23]. Dong *et al.* [6] proposes SRCNN which is a shallow three-layer network to map interpolated LR images to HR images. Kim *et al.* [15] proposes the VDSR network, which is composed of 20 layers and global skip-connection to improve the performance. In addition, Dong *et al.* [7] designs the transposed convolution layer, and Shi *et al.* [31] proposes the sub-pixel convolution layer for SR tasks, and both performed the upsampling operation at the end of the CNN and hence largely saved on computation in the feature extraction phase due to the reduction of spatial dimension. Lim *et al.* [20] has proposes EDSR and MDSR, which remove Batch Normalization layers in SRResnet [18] and greatly improve the performance. Zhang *et al.* [46] proposes RDN networks by introducing dense connections into EDSR residual blocks. RCAN [45] introduces channel attention to achieve better SR performance. However, most of these CNN-based methods contain large parameters and require large amounts of computation, which limits their real-world applications.

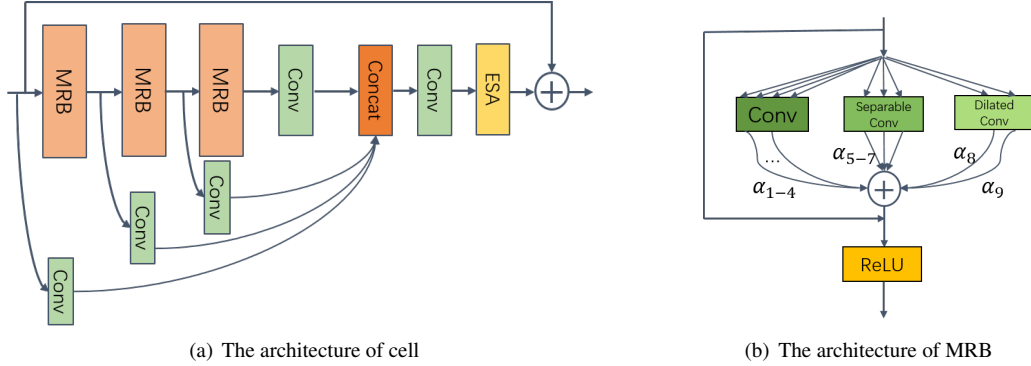


Figure 2. The cell-level search space. The cell is composed of 3 mixed residual blocks with an information distillation mechanism and an ESA block. The ‘Conv’ in figure(a) denotes the 1×1 convolution layer that cuts the channel number by half. Figure(b) shows the architecture of mixed block, which is composed of multiple operations weighted by parameter α , residual skip connection, and ReLU layer.

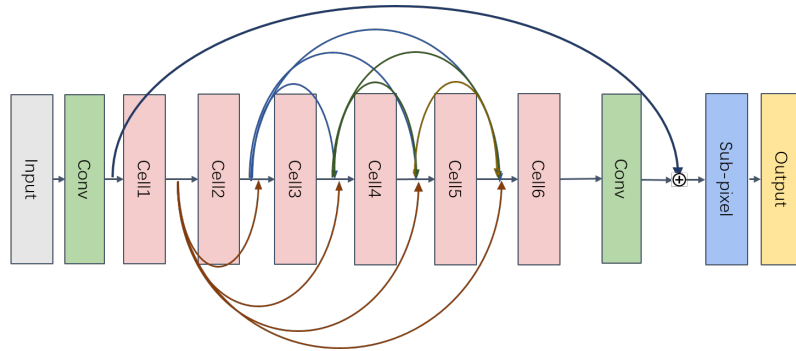


Figure 3. The network-level search space. Each cell is connected with all of its prior cells. And each connection is weighted by architecture parameter β . Each cell’s input feature is composed of weighted features from the prior cells through concatenation and 1×1 convolution. The connections from each cell to the last convolution layer are omitted for clarity.

2.2. Lightweight Image Super-Resolution

Lightweight and efficient CNN for SR tasks has been widely explored to suit mobile devices with an extremely small amount of parameters and computation [33, 2, 14, 13, 48, 24, 42, 22]. In order to reduce the parameters, Kim *et al.* [33] introduces recursive layers combined with residual schemes in the feature extraction stage. Ahn *et al.* [2] proposes the CARN-M model which utilizes group convolution and cascade network architecture that significantly reduces the parameters. Hui *et al.* [14, 13] proposes an information distillation mechanism (IDM) that utilized a channel splitting strategy to distill and compress local short-path feature information. RFDN [22] rethinks the channel splitting strategy and decouples the convolution layer and channel splitting layer. Furthermore, they apply the skip-connection on the 3×3 convolution that makes up the shallow residual block (SRB), which significantly improves the SR performance. For this they won first place in the AIM2020 efficient super-resolution challenge.

2.3. SISR with Neural Architecture Search

As NAS techniques have achieved great success in image classification [21, 10] and other tasks, recent works

have started to adopt NAS to search efficient SR networks. FALSr [5] utilizes reinforcement learning and evolutionary methods to search for lightweight SR models, building SR as a constrained multi-objective optimization problem. Song *et al.* [32] proposes to search for multiple handcrafted efficient residual dense blocks to stack the SR model using evolutionary methods. Guo *et al.* [9] proposes to search for cell structures and upsampling positions with reinforcement learning. Recently, TPSR [19] has adopted reinforcement learning to find an efficient GAN-based SR model, resulting a tiny SR model that performs well on both perceptual and distortion metrics. However, most of the prior SR methods with NAS utilized reinforcement learning or evolutionary methods that were time-consuming. In this work, we explore the fully differentiable NAS to search for an efficient, accurate, and lightweight SR model with a single GPU.

3. Method

In this section, we introduce our Differentiable NAS method for Lightweight Super-Resolution model, dubbed DLSR. Below, we first describe the search space of cell-level and network-level. Then, we discuss the search strategy and loss function of our proposed DLSR.

Table 1. Operations and their complexities in mixed layer. Dilated convolution [40] is joint with group convolution. Multi-Adds are calculated in $\times 2$ SR task with 50 channels on 1280 \times 720 image.

Operation	Kernel Size	Params (K)	Muti-Adds (G)
convolution	1 \times 1	2.5	0.576
	3 \times 3	22.5	5.184
	5 \times 5	62.5	14.400
	7 \times 7	122.5	28.224
Separable convolution	3 \times 3	5.9	1.359
	5 \times 5	7.5	1.728
	7 \times 7	9.9	2.281
Dilated convolution	3 \times 3	2.95	0.680
	5 \times 5	3.75	0.864

3.1. Search Space

Cell-level search space The cell-level topology structure is based on residual feature distillation block (RFDB) [22], which is comprised of three shallow residual blocks (SRB) with an information distillation mechanism and a contrast-aware channel attention (CCA) layer [13]. The smallest building block SRB is composed of a 3 \times 3 convolution layer and a residual connection. However, we argue that the 3 \times 3 convolution in RFDB could be suboptimal and would thus not always be the best choice for lightweight super-resolution. In order to improve the flexibility of the RFDB and search for a more lightweight structure, we replace the SRB with **Mixed Residual Block (MRB)** in Figure 2. The MRB is composed of a mixed layer, a residual connection, and a ReLU layer, in which the mixed layer is made up of multiple operations including separable convolution, dilated convolution, and normal convolution, as shown in Table 3.1. For mixed layer k , we denote the input feature as x_k , and the operation space as O , where each element represents a candidate function $o(\cdot)$ weighted by the cell architecture parameters α_o^k , as illustrated in Figure 2. We use softmax to perform the continuous relaxation of the operation space as done in Darts [21]. Thus, the output of mixed layer k denoted by $f_k(x_k)$ is given as:

$$f_k(x_k) = \sum_{o \in O} \frac{\exp(\alpha_o^k)}{\sum_{o' \in O} \exp(\alpha_{o'}^k)} o(x^k). \quad (1)$$

During searching, the operation with the largest α_o^k is reserved as the genotype of the layer. The structure of each cell is composed of three MRBs with a feature distillation mechanism and an enhanced spatial attention (ESA) block as shown in Figure 2. Hence, the number of possible combinations for each cell is 9 \times 9 \times 9.

Network-level search space Different from HNAS [9] which designs the network-level search space to search for the upsampling positions or HiNAS [41] that is designed to search for the network width, we design the network-level search space to search for the shortcut connections among the cells to explore the intermediate information, as shown in Figure 3. The whole network is stacked with 6 cells, and each cell is connected with all of its predecessors. The output features of its prior cells are concatenated and passed

into 1 \times 1 convolution layer to aggregate the information. In addition, each cell’s output feature is connected to the last convolution layer. The connection between cell i and cell j , which is also the feature maps of cell i , is denoted x^i , weighted by the network-level architecture parameters $\beta^{(i,j)}$. We also utilize softmax function as continuous relaxation for parameters $\beta^{(i,j)}$ as Eq. (1). Then, the input of the cell j denoted by I_j is formulated as:

$$I_j = g \left(\frac{\exp(\beta^{(i,j)})}{\sum_{i' < j} \exp(\beta^{(i',j)})} x^i \right), \quad (2)$$

where $g(\cdot)$ denotes the operations of concatenation and 1 \times 1 convolution. Thus, we build a continuous and dense super-network search space considering all the intermediate information among the cells.

Search complexity Based on the above illustration, the proposed DLSR method includes both the cell-level and network-level search spaces. Thus, the overall search complexity of our method is estimated as:

$$9 \times 9 \times 9 \times 5 \times 4 \times 3 \times 2 = 87480. \quad (3)$$

It is nontrivial and requires a large amount of computation cost to explore such a large search space for a lightweight and accurate super-resolution model via reinforcement learning [9] or evolutionary algorithm [5, 32] based neural architecture search approaches. In this work, we solve this problem via a fully differentiable neural architecture search approach.

3.2. Search Strategy

We extend the popular differentiable NAS methods including DARTS [21] and its improved version MiLeNas [10] for the low-level computer vision (SISR) task. These two methods were originally proposed for the image classification task which is a high-level computer vision task. Motivated by MiLeNas, the objective function of our DLSR model is defined as the following regularized form:

$$\min_{\theta, \alpha, \beta} [L_{tr}(\theta^*(\alpha, \beta) + \lambda L_{val}(\theta^*(\alpha, \beta); \alpha, \beta))], \quad (4)$$

where θ denotes the weights parameters of the network and λ is a non-negative regularization parameter that balances the importance of the training loss and validation loss. Because the architecture parameters α and β are both continuous, we directly apply Adam [17] to solve problem (4). We define the architecture parameter $A = [\alpha, \beta]$, the parameters θ , α , and β are updated via the following iteration:

$$\theta = \theta - \eta_{\theta} \nabla_{\theta} L_{tr}(\theta, A); \quad (5)$$

$$A = A - \eta_A \nabla_A L_{tr}(\theta, A) + \lambda \nabla_A L_{val}(\theta, A). \quad (6)$$

During the searching process, we preserve the operation that has the maximal value of the α as the searched operation of the layer. The connections that have the maximal and the

submaximal value of the β are preserved as the searched input connections of the cell. Our searching and training procedure is summarized in Algorithm 1.

3.3. Loss Function

To achieve lightweight and accurate SR models, the loss function is composed of three parts, which include L1 loss as distortion loss, HFEN loss [28] for reconstruction, and parameters of the operations as a lightweight limitation.

$$L_1 = \frac{1}{N} \sum_{i=1}^N |H_\theta(I^{LR}) - I^{HR}| \quad (7)$$

$$L_{HFEN} = \frac{1}{N} \sum_{i=1}^N |\nabla H_\theta(I^{LR}) - \nabla I^{HR}| \quad (8)$$

$$L_P = \sum_{o \in O} \frac{p_o}{\sum_{c \in O} p_c} softmax(\alpha_o) \quad (9)$$

$$L(\theta) = L_1 + \mu \times L_{HFEN} + \gamma \times L_P. \quad (10)$$

Specifically, L_1 loss is popularly used for SR tasks [20, 5, 22, 47] to minimize the distortion between the reconstructed SR image and ground truth HR image; L_{HFEN} [4] is a gradient-domain L1 loss, and each gradient $\nabla(\cdot)$ is computed using High Frequency Error Norm (HFEN) [28] which is an image comparison metric from medical imaging and uses a Laplacian of Gaussian kernel for edge-detection with Gaussian filter pre-smoothed images. L_{HFEN} is adopted to strengthen the reconstruction of image details such as edges and stripes. L_P is a regularization item based on the parameters of operations. p_o denotes the number of parameters of operation o . L_P utilizes the number of the parameters to weigh the architecture parameter α , so as to reduce the α of the operations which have a large number of parameters and push the algorithm to search for lightweight operations. The μ and γ are weighting parameters for balancing the reconstruction performance and model complexity, respectively. As for retraining the searched networks, the last term $L(\theta)$ in the total loss function (10) is removed by setting $\gamma = 0$.

4. Experiments

4.1. Datasets

We use high-quality DIV2K [1] and Flickr2K [35] datasets as training datasets. The DIV2K dataset consists of 800 training images and the Flickr2K dataset consists of 2650 training images. The LR images are obtained by the bicubic downsampling of HR images. In addition, we use the standard benchmark datasets, Set5 [3], Set14 [39], B100 [26], and Urban100 [12] as test datasets.

4.2. Implementation Details

We merge the DIV2K and Flickr2K datasets together and denote them as DF2K dataset with a total of 3450 images.

Algorithm 1: Searching and training Algorithm

Input: Training set \mathbb{D}

- 1 Initialize the super-network \mathcal{T} with architecture parameters α and β .
- 2 Split training set \mathbb{D} into \mathbb{D}_{train} and \mathbb{D}_{valid} .
- 3 Train the super-network \mathcal{T} on \mathbb{D}_{train} for several steps to warm up.
- 4 **for** $t = 1, 2, \dots, T$ **do**
- 5 Sample train batch $\mathbb{B}_t = \{(x_i, y_i)\}_{i=1}^{batch}$ from \mathbb{D}_{train}
- 6 Optimize θ on the \mathbb{B}_t by Eq. (5)
- 7 Sample valid batch $\mathbb{B}_v = \{(x_i, y_i)\}_{i=1}^{batch}$ from \mathbb{D}_{valid}
- 8 Optimize α and β on the \mathbb{B}_v by Eq. (6)
- 9 Save the genotypes of the searched networks
- 10 Train searched networks from the scratch
- 11 Pick up the best performing network \mathcal{S}

Output: A lightweight SR network \mathcal{S}

During the searching stage, we split the dataset to 3000 images as training dataset \mathbb{D}_{train} and the remaining 450 images as validation dataset \mathbb{D}_{valid} . We augment the datasets by random rotations of 90° , 180° , 270° , and horizontal flips. We perform $\times 2$ SR for searching the neural network architectures and apply the searched models to $\times 2$, $\times 3$, $\times 4$ SR tasks. Both the searching and training stages are performed on a single NVIDIA Tesla V100 GPU. More implementation details can be found in **supplementary material**.

4.3. Searched Results

The searched network structure and cell structure are shown in Figure 4. For clarity, we omit the connections between each block and the end of the model in the figure. The searched cell is made up of a 1×1 convolution layer, 7×7 separable convolution layer, 5×5 separable convolution layer, ESA block, and residual connections with information distillation mechanism. Since the parameters and FLOPS of the 1×1 convolution, 5×5 separable convolution, and 7×7 separable convolution are all fewer than the original 3×3 convolution, we obtain a much smaller (nearly half the original size) model compared with vanilla RFDN [22].

4.4. Comparison with State-of-the-art Methods

We compare the DLSR model with state-of-the-art lightweight SR methods on two commonly-used metrics: peak signal-to-noise ratio (PSNR) and structural similarity index measure (SSIM) [38] on the Y channel of the transformed YCbCr space. We also present the number of the parameters and number of the operations (Multi-Adds) to show the model complexity. Multi-Adds is calculated on 720p (1280×720) HR images. The $\times 2$, $\times 3$, $\times 4$ super-

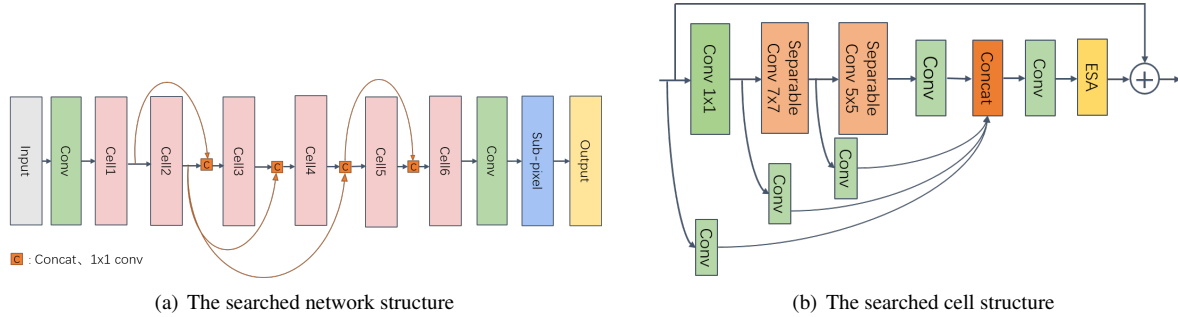


Figure 4. The searched network and cell structures. The connections from each cell to the last convolution layer is omitted for clarity.

Table 2. Image super-resolution results with scale factors of 2, 3, 4 on benchmark datasets.

Method	Scale	Params (K)	Multi-Adds (G)	Set5	Set14	B100	Urban100
				PSNR/SSIM	PSNR/SSIM	PSNR/SSIM	PSNR/SSIM
Bicubic	×2	-	-	33.66/0.9299	30.24/0.8688	29.56/0.8403	26.88/0.8403
DRRN [33]		297	6,796.9	37.74/0.9591	33.23/0.9136	32.05/0.8973	31.23/0.9188
CARN-M [2]		412	91.2	37.53/0.9583	33.26/0.9141	31.92/0.8960	31.23/0.9194
FALSR-B [5]		326	74.7	37.61/0.9585	33.29/0.9143	31.97/0.8967	31.28/0.9191
ESRN-V [32]		324	73.4	37.85/0.9600	33.42/0.9161	32.10/0.8987	31.79/0.9248
IMDN [13]		694	-	38.00/0.9605	33.63/0.9177	32.19/0.8996	32.17/0.9283
PAN [47]		261	70.5	38.00/0.9605	33.59/0.9181	32.18/0.8997	32.01/0.9273
RFDN [23]		534	123.0	38.05/0.9606	33.68/0.9184	32.16/0.8994	32.12/0.9278
DLSR(Ours)		322	68.1	38.04/0.9606	33.67/0.9183	32.21/0.9002	32.26/0.9297
Bicubic		×3	-	-	30.39/0.8682	27.55/0.7742	27.21/0.7385
DRRN [33]	297		6,796.9	34.03/0.9244	29.96/0.8349	28.95/0.8004	27.53/0.8378
CARN-M [2]	412		46.1	33.99/0.9236	30.08/0.8367	28.91/0.8000	27.55/0.8385
ESRN-V [32]	324		36.2	34.23/0.9262	30.27/0.8400	29.03/0.8039	27.95/0.8481
IMDN [13]	703		-	34.36/0.9270	30.32/0.8417	29.09/0.8046	28.17/0.8519
PAN [47]	261		39.0	34.40/0.9271	30.36/0.8423	29.11/0.8050	28.11/0.8511
RFDN [23]	541		55.4	34.41/0.9273	30.34/0.8420	29.09/0.8050	28.21/0.8525
DLSR(Ours)	329		30.9	34.49/0.9279	30.39/0.8428	29.13/0.8061	28.26/0.8548
Bicubic	×4	-	-	28.42/0.8104	26.00/0.7027	25.96/0.6675	23.14/0.6577
DRRN [33]		297	6,796.9	31.68/0.8888	28.21/0.7720	27.38/0.7284	25.44/0.7638
CARN-M [2]		412	32.5	31.92/0.8903	28.42/0.7762	27.44/0.7304	25.62/0.7694
ESRN-V [32]		324	20.7	31.99/0.8919	28.49/0.7779	27.50/0.7331	25.87/0.7782
IMDN [13]		715	-	32.21/0.8948	28.58/0.7811	27.56/0.7353	26.04/0.7838
PAN [47]		272	28.2	32.13/0.8948	28.61/0.7822	27.59/0.7363	26.11/0.7854
RFDN [23]		550	31.6	32.24/0.8952	28.61/0.7819	27.57/0.7360	26.11/0.7858
DLSR(Ours)		338	17.9	32.33/0.8963	28.68/0.7832	27.61/0.7374	26.19/0.7892

resolution results are shown in Table 2, and the best results are highlighted. The visual performance of $\times 2$, $\times 4$ super-resolution are shown in Figures 5 and 6. Compared with DRRN [33], our method only takes 1% Multi-Adds, while achieving 1dB PSNR improvement on the Urban100 dataset in $\times 2$, $\times 3$ SR tasks, 0.7dB PSNR improvement on the Set5 dataset in $\times 4$ SR task, as well as 0.3-0.7dB PSNR improvement on other tasks, respectively. Our method surpasses other NAS based methods like FALSR-B [5] and ESRN-V [32] by a large margin with 0.2-0.4dB PSNR improvement with fewer parameters and Multi-Adds in most of the SR tasks (Table 2). As shown in Table 4, the search cost of our method is significantly less than NAS-based SR methods. FALSR-B [5] takes less than 3 days on 8 GPUs to execute

their pipeline once. ESRN-V [32] takes around one day on 8 GPUs to execute their evolution procedure. Our method only takes around 2 days on one GPU.

Compared with hand-crafted light-weight models like IMDN [13] and RFDN [22], the DLSR method only takes about half the amount of parameters while still outperforming them. Compared with PAN [47], which is the most lightweight deep SR model in AIM2020 Efficient Super Resolution, our method is still able to outperform it with fewer Multi-Adds.

Table 4. Searching cost of NAS based SR methods

NAS based SR method	GPU days
FALSR [5]	24
ESRN [32]	8
DLSR(ours)	2

Table 3. Comparison results with TPSR-NOGAN on benchmark datasets.

Method	Scale	Params (K)	Multi-Adds (G)	Set5	Set14	B100	Urban100
				PSNR/SSIM	PSNR/SSIM	PSNR/SSIM	PSNR/SSIM
TPSR-NOGAN	$\times 2$	60	14.0	37.38/0.9583	33.00/0.9123	31.75/0.8942	30.61/0.9119
DLSR-S(Ours)	$\times 2$	56	12.4	37.71/0.9595	33.33/0.9150	31.96/0.8973	31.26/0.9196
TPSR-NOGAN	$\times 4$	61	3.6	31.10/0.8779	27.95/0.7663	27.15/0.7214	24.97/0.7456
DLSR-S(Ours)	$\times 4$	62	3.4	31.75/0.8885	28.31/0.7745	27.38/0.7298	25.47/0.7663

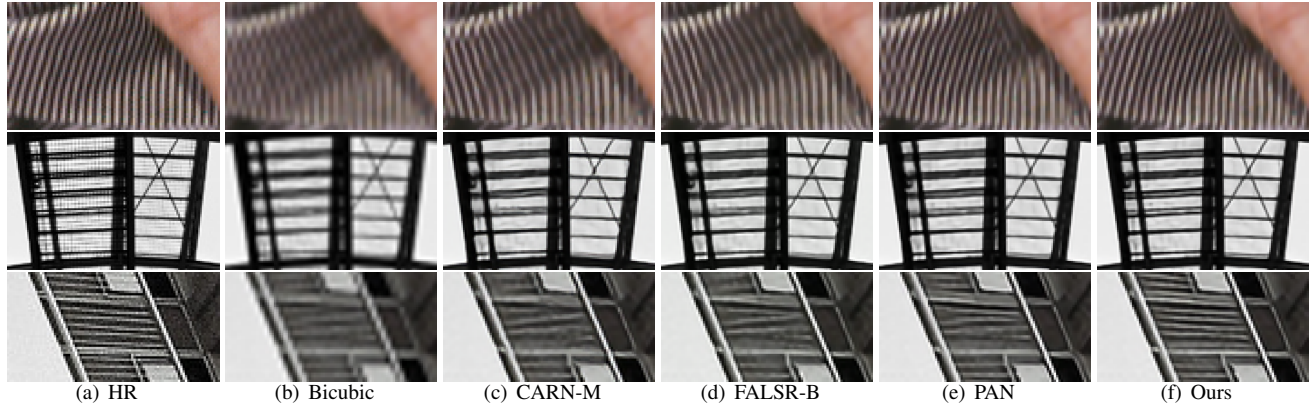


Figure 5. Visual comparisons among SOTA lightweight models in $\times 2$ image super-resolution. The test image patches are from Set14 and Urban100. Note that the results of FALS-R-B are based on our test with the pre-trained model which is released by the authors. The results of CARN-M and PAN are directly taken from the authors’ release. Our method has better reconstruction performance on image details, such as thin stripes on the clothes and edges of windows.

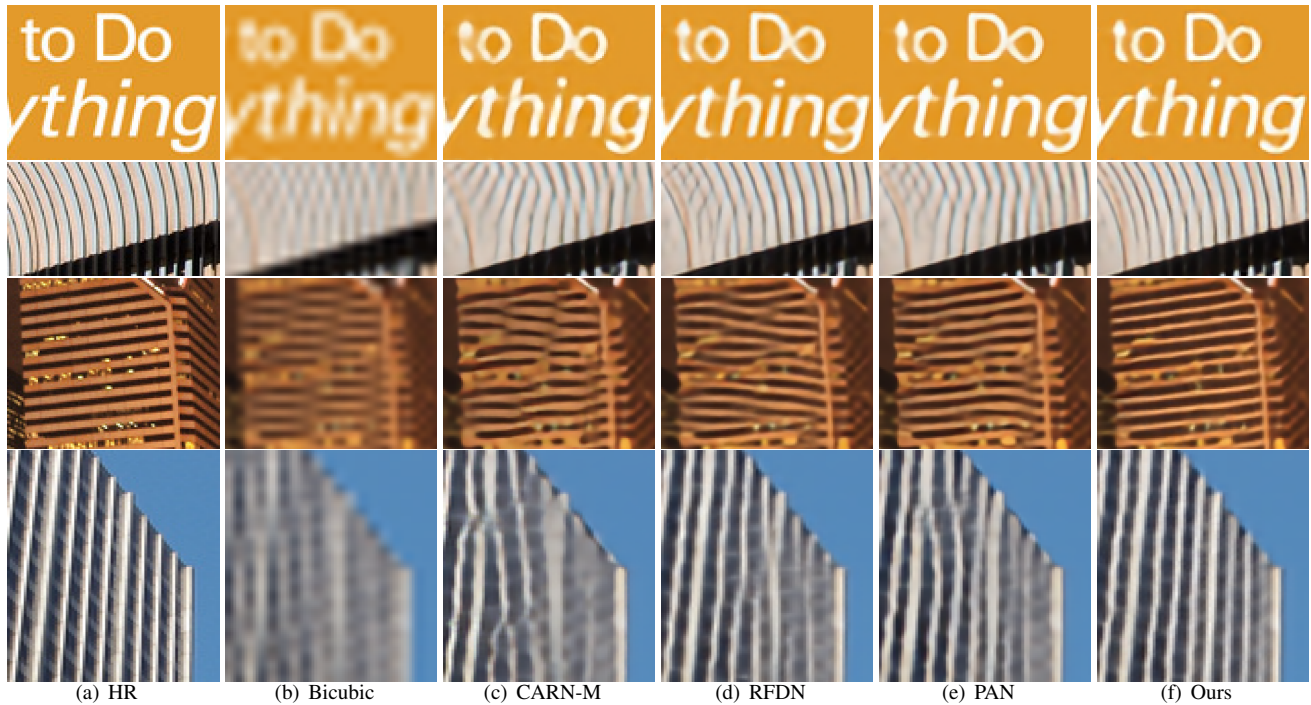


Figure 6. Visual comparisons among SOTA lightweight models in $\times 4$ image super-resolution. The test image patches are from Set14 and Urban100. Note that the results of RFDN are based on our test with the pre-trained model which is officially released by the authors. Our method shows better reconstruction performance and less deformation on image details such as texts and stripes.

The visual comparison results show that our method achieves better performance in reconstructing image details such as tiny stripes and the edges of the text. In Figure 5, our DLSR method reconstructs the right direction of the

thin stripes on the clothes with high visual quality and successfully reconstructs the edge of the window, while other methods cannot. In Figure 6, our method reconstructs the round edge of the text ‘O’ and other stripe-like image details

Table 5. Comparison results between the model with/without network-level connections DLSR/DLSR-B.

Method	Scale	Set5	Set14	B100	Urban100
		PSNR/SSIM	PSNR/SSIM	PSNR/SSIM	PSNR/SSIM
DLSR-B	$\times 2$	38.04/0.9606	33.63/0.9177	32.20/0.9000	32.20/0.9293
DLSR	$\times 2$	38.04/0.9606	33.67/0.9183	32.21/0.9002	32.26/0.9297
DLSR-B	$\times 4$	32.27/0.8959	28.67/0.7832	27.60/0.7372	26.16/0.7885
DLSR	$\times 4$	32.33/0.8963	28.68/0.7832	27.61/0.7374	26.19/0.7892

Table 6. Comparison results with different loss function configurations on benchmark datasets.

Method	Scale	Params (K)	Multi-Adds (G)	Set5	Set14	B100	Urban100
				PSNR/SSIM	PSNR/SSIM	PSNR/SSIM	PSNR/SSIM
DLSR-L1	$\times 2$	323	68.1	38.04/0.9606	33.69/0.9185	32.20/0.9002	32.27/0.9297
DLSR-HFEN	$\times 2$	365	77.8	38.02/0.9605	33.78/0.9200	32.21/0.9003	32.34/0.9305
DLSR	$\times 2$	322	68.1	38.04/0.9606	33.67/0.9183	32.21/0.9002	32.26/0.9297

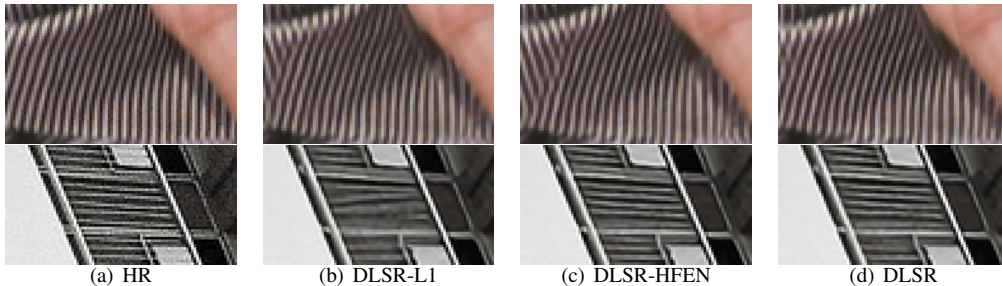


Figure 7. Visual comparisons among the models trained with different loss configurations in $\times 2$ image super-resolution. DLSR-L1 model is searched and retrained only with L1 loss. DLSR-HFEN model is searched and retrained with L1 loss and HFEN loss. DLSR model is searched and retrained with L1 loss, HFEN loss, and parameter regularization.

without distortion. In summary, the quantitative and visual results both demonstrate that our models outperform the state-of-the-art SR models on multiple datasets and scales with fewer parameters and Multi-Adds.

In addition, to compare our method with the Tiny Perceptual Super Resolution (TPSR) model [19], which is a super lightweight SR model with 60K parameters, we cut the channel number of our DLSR model to 18 and denote the smaller model as DLSR-S. The $\times 2$, $\times 4$ SR comparison result is shown in Table 3. As our method is not based on the generative adversarial networks (GAN), we compare it with the baseline model of the TPSR method called TPSR-NOGAN. The result indicates that even with fewer Multi-Adds, our DLSR-S model can still surpass the TPSR-NOGAN with a large margin of PSNR and SSIM.

4.5. Ablation Studies

First, we discuss the effectiveness of network-level connections. To compare with DLSR, we design our method to search for a baseline model only on the cell-level search space. After searching and retraining, we name this model DLSR-B. Coincidentally, the DLSR-B has the same numbers of parameters and Multi-Adds as DLSR. The comparison result is illustrated in Table 5. The result shows that the network-level connections can improve the performance of DLSR-B. Thus, the search space of network-level connections which we propose is innovative and meaningful.

Second, we discuss the effectiveness of the loss function we designed that is comprised of three parts: the L1 loss, the HFEN loss, and the parameter loss. We conduct the experiments on three different models: DLSR-L1, DLSR-HFEN, DLSR. The DLSR-L1 model is searched and retrained only with L1 loss. The DLSR-HFEN model is searched and retrained with L1 loss and HFEN loss. The DLSR model is searched and retrained on all three parts of the loss. The comparison result is illustrated in Table 6 and Figure 7. The result shows the DLSR model achieves a better trade-off between the SR performance and the model complexity, and that HFEN loss can contribute to a better visual effect with sharper image details.

In addition, more visual comparisons and ablation studies on verifying the search stability of our DLSR model can be found in **supplementary material**.

5. Conclusions

In this work, we propose a novel Differentiable neural architecture search approach to search for Lightweight single image Super-Resolution models on both the cell-level and the network-level, dubbed DLSR. In addition, we design a novel loss function that considers distortion, high-frequency reconstruction, and lightweight regularization that jointly pushes the searching direction to explore a better lightweight SR model. Experimental results show that our DLSR method can surpass both the hand-crafted

and NAS-based SOTA lightweight SR methods in terms of PSNR and SSIM with fewer parameters and Multi-Adds.

References

- [1] Eirikur Agustsson and Radu Timofte. Ntire 2017 challenge on single image super-resolution: Dataset and study. In *Proceedings of the IEEE Conference on Computer Vision and Pattern Recognition Workshops*, pages 126–135, 2017. 5
- [2] Namhyuk Ahn, Byungkon Kang, and Kyung-Ah Sohn. Fast, accurate, and lightweight super-resolution with cascading residual network. In *Proceedings of the European Conference on Computer Vision (ECCV)*, pages 252–268, 2018. 1, 3, 6
- [3] Marco Bevilacqua, Aline Roumy, Christine Guillemot, and Marie Line Alberi-Morel. Low-complexity single-image super-resolution based on nonnegative neighbor embedding. 2012. 1, 2, 5
- [4] Chakravarty R Alla Chaitanya, Anton S Kaplanyan, Christoph Schied, Marco Salvi, Aaron Lefohn, Derek Nowrouzezahrai, and Timo Aila. Interactive reconstruction of monte carlo image sequences using a recurrent denoising autoencoder. *ACM Transactions on Graphics (TOG)*, 36(4):1–12, 2017. 5
- [5] Xiangxiang Chu, Bo Zhang, Hailong Ma, Ruijun Xu, and Qingyuan Li. Fast, accurate and lightweight super-resolution with neural architecture search. *arXiv preprint arXiv:1901.07261*, 2019. 1, 2, 3, 4, 5, 6
- [6] Chao Dong, Chen Change Loy, Kaiming He, and Xiaoou Tang. Image super-resolution using deep convolutional networks. *IEEE transactions on pattern analysis and machine intelligence*, 38(2):295–307, 2015. 1, 2
- [7] Chao Dong, Chen Change Loy, and Xiaoou Tang. Accelerating the super-resolution convolutional neural network. In *European conference on computer vision*, pages 391–407. Springer, 2016. 2
- [8] Yong Guo, Jian Chen, Jingdong Wang, Qi Chen, Jiezhong Cao, Zeshuai Deng, Yanwu Xu, and Mingkui Tan. Closed-loop matters: Dual regression networks for single image super-resolution. In *Proceedings of the IEEE/CVF Conference on Computer Vision and Pattern Recognition*, pages 5407–5416, 2020. 1
- [9] Yong Guo, Yongsheng Luo, Zhenhao He, Jin Huang, and Jian Chen. Hierarchical neural architecture search for single image super-resolution. *IEEE Signal Processing Letters*, 27:1255–1259, 2020. 3, 4
- [10] Chaoyang He, Haishan Ye, Li Shen, and Tong Zhang. Milenas: Efficient neural architecture search via mixed-level reformulation. In *Proceedings of the IEEE/CVF Conference on Computer Vision and Pattern Recognition*, pages 11993–12002, 2020. 3, 4
- [11] Gao Huang, Zhuang Liu, Laurens Van Der Maaten, and Kilian Q Weinberger. Densely connected convolutional networks. In *Proceedings of the IEEE conference on computer vision and pattern recognition*, pages 4700–4708, 2017. 2
- [12] Jia-Bin Huang, Abhishek Singh, and Narendra Ahuja. Single image super-resolution from transformed self-exemplars. In *Proceedings of the IEEE conference on computer vision and pattern recognition*, pages 5197–5206, 2015. 2, 5
- [13] Zheng Hui, Xinbo Gao, Yunchu Yang, and Xiumei Wang. Lightweight image super-resolution with information multi-distillation network. In *Proceedings of the 27th ACM International Conference on Multimedia (ACM MM)*, pages 2024–2032, 2019. 1, 3, 4, 6
- [14] Zheng Hui, Xiumei Wang, and Xinbo Gao. Fast and accurate single image super-resolution via information distillation network. In *Proceedings of the IEEE conference on computer vision and pattern recognition*, pages 723–731, 2018. 3
- [15] Jiwon Kim, Jung Kwon Lee, and Kyoung Mu Lee. Accurate image super-resolution using very deep convolutional networks. In *Proceedings of the IEEE Conference on Computer Vision and Pattern Recognition (CVPR)*, June 2016. 1, 2
- [16] Jiwon Kim, Jung Kwon Lee, and Kyoung Mu Lee. Deeply-recursive convolutional network for image super-resolution. In *Proceedings of the IEEE conference on computer vision and pattern recognition*, pages 1637–1645, 2016. 1
- [17] Diederik P Kingma and Jimmy Ba. Adam: A method for stochastic optimization. *arXiv preprint arXiv:1412.6980*, 2014. 4, 11
- [18] Christian Ledig, Lucas Theis, Ferenc Huszár, Jose Caballero, Andrew Cunningham, Alejandro Acosta, Andrew Aitken, Alykhan Tejani, Johannes Totz, Zehan Wang, et al. Photo-realistic single image super-resolution using a generative adversarial network. In *Proceedings of the IEEE conference on computer vision and pattern recognition*, pages 4681–4690, 2017. 1, 2
- [19] Royson Lee, Łukasz Dudziak, Mohamed Abdelfattah, Stylianos I Venieris, Hyeji Kim, Hongkai Wen, and Nicholas D Lane. Journey towards tiny perceptual super-resolution. In *European Conference on Computer Vision*, pages 85–102. Springer, 2020. 1, 3, 8
- [20] Bee Lim, Sanghyun Son, Heewon Kim, Seungjun Nah, and Kyoung Mu Lee. Enhanced deep residual networks for single image super-resolution. In *The IEEE Conference on Computer Vision and Pattern Recognition (CVPR) Workshops*, pages 136–144, 2017. 1, 2, 5
- [21] Hanxiao Liu, Karen Simonyan, and Yiming Yang. Darts: Differentiable architecture search. *arXiv preprint arXiv:1806.09055*, 2018. 2, 3, 4
- [22] Jie Liu, Jie Tang, and Gangshan Wu. Residual feature distillation network for lightweight image super-resolution. *arXiv preprint arXiv:2009.11551*, 2020. 1, 2, 3, 4, 5, 6
- [23] Jie Liu, Wenjie Zhang, Yuting Tang, Jie Tang, and Gangshan Wu. Residual feature aggregation network for image super-resolution. In *Proceedings of the IEEE/CVF Conference on Computer Vision and Pattern Recognition*, pages 2359–2368, 2020. 1, 2, 6
- [24] Xiaotong Luo, Yuan Xie, Yulun Zhang, Yanyun Qu, Cuihua Li, and Yun Fu. Latticenet: Towards lightweight image super-resolution with lattice block. In Andrea Vedaldi, Horst Bischof, Thomas Brox, and Jan-Michael Frahm, editors, *Computer Vision – ECCV 2020*, pages 272–289, Cham, 2020. Springer International Publishing. 3

- [25] Cheng Ma, Yongming Rao, Yean Cheng, Ce Chen, Jiwen Lu, and Jie Zhou. Structure-preserving super resolution with gradient guidance. In *Proceedings of the IEEE/CVF Conference on Computer Vision and Pattern Recognition*, pages 7769–7778, 2020. 1
- [26] David Martin, Charless Fowlkes, Doron Tal, and Jitendra Malik. A database of human segmented natural images and its application to evaluating segmentation algorithms and measuring ecological statistics. In *Proceedings Eighth IEEE International Conference on Computer Vision. ICCV 2001*, volume 2, pages 416–423. IEEE, 2001. 2, 5
- [27] Zhihong Pan, Baopu Li, Teng Xi, Yanwen Fan, Gang Zhang, Jingtuo Liu, Junyu Han, and Errui Ding. Real image super resolution via heterogeneous model ensemble using gp-nas. In *European Conference on Computer Vision*, pages 423–436. Springer, 2020. 1
- [28] Saiprasad Ravishankar and Yoram Bresler. Mr image reconstruction from highly undersampled k-space data by dictionary learning. *IEEE transactions on medical imaging*, 30(5):1028–1041, 2010. 2, 5
- [29] George Seif and Dimitrios Androutsos. Large receptive field networks for high-scale image super-resolution. In *Proceedings of the IEEE Conference on Computer Vision and Pattern Recognition Workshops*, pages 763–772, 2018. 2
- [30] Taizhang Shang, Qiuju Dai, Shengchen Zhu, Tong Yang, and Yandong Guo. Perceptual extreme super-resolution network with receptive field block. In *Proceedings of the IEEE/CVF Conference on Computer Vision and Pattern Recognition Workshops*, pages 440–441, 2020. 2
- [31] Wenzhe Shi, Jose Caballero, Ferenc Huszár, Johannes Totz, Andrew P Aitken, Rob Bishop, Daniel Rueckert, and Zehan Wang. Real-time single image and video super-resolution using an efficient sub-pixel convolutional neural network. In *Proceedings of the IEEE conference on computer vision and pattern recognition*, pages 1874–1883, 2016. 2
- [32] Dehua Song, Chang Xu, Xu Jia, Yiyi Chen, Chunjing Xu, and Yunhe Wang. Efficient residual dense block search for image super-resolution. In *Proceedings of the AAAI Conference on Artificial Intelligence*, volume 34, pages 12007–12014, 2020. 1, 2, 3, 4, 6
- [33] Ying Tai, Jian Yang, and Xiaoming Liu. Image super-resolution via deep recursive residual network. In *Proceedings of the IEEE conference on computer vision and pattern recognition*, pages 3147–3155, 2017. 3, 6
- [34] Ying Tai, Jian Yang, Xiaoming Liu, and Chunyan Xu. Memnet: A persistent memory network for image restoration. In *Proceedings of the IEEE international conference on computer vision*, pages 4539–4547, 2017. 2
- [35] Radu Timofte, Eirikur Agustsson, Luc Van Gool, Ming-Hsuan Yang, and Lei Zhang. Ntire 2017 challenge on single image super-resolution: Methods and results. In *Proceedings of the IEEE conference on computer vision and pattern recognition workshops*, pages 114–125, 2017. 5
- [36] Tong Tong, Gen Li, Xiejie Liu, and Qinquan Gao. Image super-resolution using dense skip connections. In *Proceedings of the IEEE international conference on computer vision*, pages 4799–4807, 2017. 2
- [37] Xintao Wang, Ke Yu, Shixiang Wu, Jinjin Gu, Yihao Liu, Chao Dong, Yu Qiao, and Chen Change Loy. Esrgan: Enhanced super-resolution generative adversarial networks. In *Proceedings of the European Conference on Computer Vision (ECCV) Workshops*, pages 0–0, 2018. 2
- [38] Zhou Wang, Alan C Bovik, Hamid R Sheikh, and Eero P Simoncelli. Image quality assessment: from error visibility to structural similarity. *IEEE transactions on image processing*, 13(4):600–612, 2004. 2, 5
- [39] Jianchao Yang, John Wright, Thomas S Huang, and Yi Ma. Image super-resolution via sparse representation. *IEEE transactions on image processing*, 19:2861–2873, 2010. 2, 5
- [40] Fisher Yu, Vladlen Koltun, and Thomas Funkhouser. Dilated residual networks. In *Proceedings of the IEEE conference on computer vision and pattern recognition*, pages 472–480, 2017. 4
- [41] Haokui Zhang, Ying Li, Hao Chen, and Chunhua Shen. Memory-efficient hierarchical neural architecture search for image denoising. In *Proceedings of the IEEE/CVF Conference on Computer Vision and Pattern Recognition*, pages 3657–3666, 2020. 4
- [42] Kai Zhang, Martin Danelljan, Yawei Li, Radu Timofte, Jie Liu, Jie Tang, Gangshan Wu, Yu Zhu, Xiangyu He, Wenjie Xu, et al. Aim 2020 challenge on efficient super-resolution: Methods and results. In *European Conference on Computer Vision*, pages 5–40. Springer, 2020. 3
- [43] Kai Zhang, Luc Van Gool, and Radu Timofte. Deep unfolding network for image super-resolution. In *Proceedings of the IEEE/CVF Conference on Computer Vision and Pattern Recognition*, pages 3217–3226, 2020. 2
- [44] Kai Zhang, Wangmeng Zuo, and Lei Zhang. Learning a single convolutional super-resolution network for multiple degradations. In *Proceedings of the IEEE Conference on Computer Vision and Pattern Recognition*, pages 3262–3271, 2018. 2
- [45] Yulun Zhang, Kungpeng Li, Kai Li, Lichen Wang, Bineng Zhong, and Yun Fu. Image super-resolution using very deep residual channel attention networks. In *Proceedings of the European conference on computer vision (ECCV)*, pages 286–301, 2018. 1, 2
- [46] Yulun Zhang, Yapeng Tian, Yu Kong, Bineng Zhong, and Yun Fu. Residual dense network for image super-resolution. In *Proceedings of the IEEE conference on computer vision and pattern recognition*, pages 2472–2481, 2018. 1, 2
- [47] Hengyuan Zhao, Xiangtao Kong, Jingwen He, Yu Qiao, and Chao Dong. Efficient image super-resolution using pixel attention. *arXiv preprint arXiv:2010.01073*, 2020. 5, 6
- [48] Feiyang Zhu and Qijun Zhao. Efficient single image super-resolution via hybrid residual feature learning with compact back-projection network. In *Proceedings of the IEEE/CVF International Conference on Computer Vision Workshops*, pages 0–0, 2019. 3

A. Experiment Details

During the search stage, the high-resolution (HR) patch size is set as 64 and the minibatch size is set as 64. We optimize the θ , α and β parameters with ADAM optimizer [17] with 2×10^5 iterations. For parameter θ , the learning rate is set to 3×10^{-4} , the momentum parameter and exponential moving average parameter are set as (0.9,0.999) and the weight decay is set to 10^{-8} . For parameters α and β , the learning rate is set to 3×10^{-4} , the momentum parameter and exponential moving average parameter are set as (0.5,0.999) and the weight decay is set to 10^{-8} . The warm-up process takes 2×10^4 steps that only parameter θ is updated. The learning rates of the warm-up process and searching process are both set to 3×10^{-4} . We save the genotypes of the searched models at about 5×10^4 step, 10^5 step, and 1.5×10^5 step when the distribution of the architecture parameters turn stable during searching. The number of channels is set to 48 and the number of cells is set to 6. The hyper-parameter λ is set as 1.0, μ is set as 0.2, and γ is set as 0.2.

For retraining the searched networks, we use the whole DF2K dataset with the same data augmentation as the searching stage. For $\times 2$, $\times 3$, $\times 4$ super-resolution, HR patch size is set as 128, 192, and 256, respectively. We train our searched DLSR model with ADAM optimizer [17] with the same settings as the optimization of the parameter θ during the searching stage. We train the model in 2×10^6 steps and set the minibatch size as 32. The learning rate is initialized with 3×10^{-4} and halved every 4×10^5 steps. The weights of both $\times 3$, $\times 4$ super-resolution models are warmed up by the weight of the pre-trained $\times 2$ SR model. All the experiments are conducted in PyTorch 1.2 and Python 3.7.

B. Ablation Study

In this section, we discuss the search stability of our method. To prove of the effectiveness of our proposed DLSR method, we repeat the searching algorithm several times with different initialization of random seed, and retrain the searched models, denoted as DLSR-a, DLSR-B, and DLSR-c. Table B shows the SR results of the lightweight SR models we have obtained. The results show that our proposed DLSR method is stable and effective.

Method	Scale	Params (K)	Multi-Adds (G)	Set5	Set14	B100	Urban100
				PSNR/SSIM	PSNR/SSIM	PSNR/SSIM	PSNR/SSIM
DLSR-a	$\times 2$	309	65	38.04/ 0.9606	33.68 /0.9181	32.20/0.9000	32.21 /0.9290
DLSR-b	$\times 2$	328	69.3	38.04/ 0.9606	33.65/0.9180	32.21 / 0.9002	32.20/0.9290
DLSR-c	$\times 2$	341	72.5	38.05 /0.9605	33.68 / 0.9183	32.19/0.9000	32.21 / 0.9292

Table 7. The results of the lightweight SR models we have searched with different initialization of random seed.

C. More Visual Comparison Results

More visual comparison results show that our DLSR model has superior performance compared with other lightweight SR models on image details. In Figure 8 and Figure 9, our method reconstructs the stripe-like and lattice-like image details on the buildings without distortion.

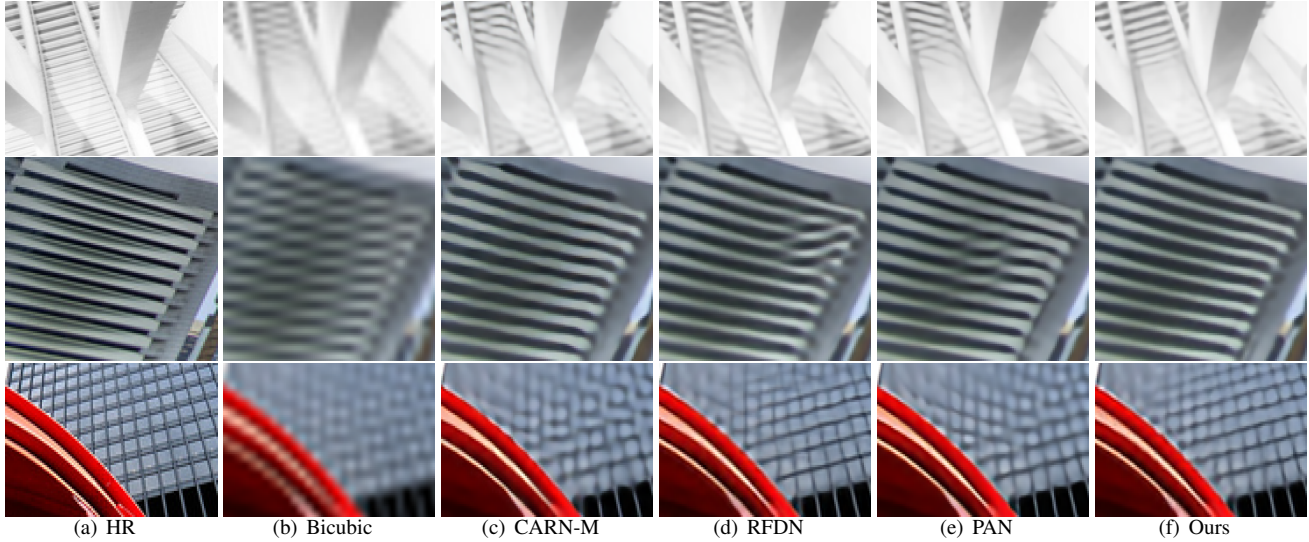


Figure 8. Visual comparisons among SOTA lightweight models in $\times 4$ image super-resolution. The test image patches are from Urban100. Note that the results of RFDN are based on our test with the pre-trained model which is officially released by the authors. Our method shows better reconstruction performance and less deformation on image details.

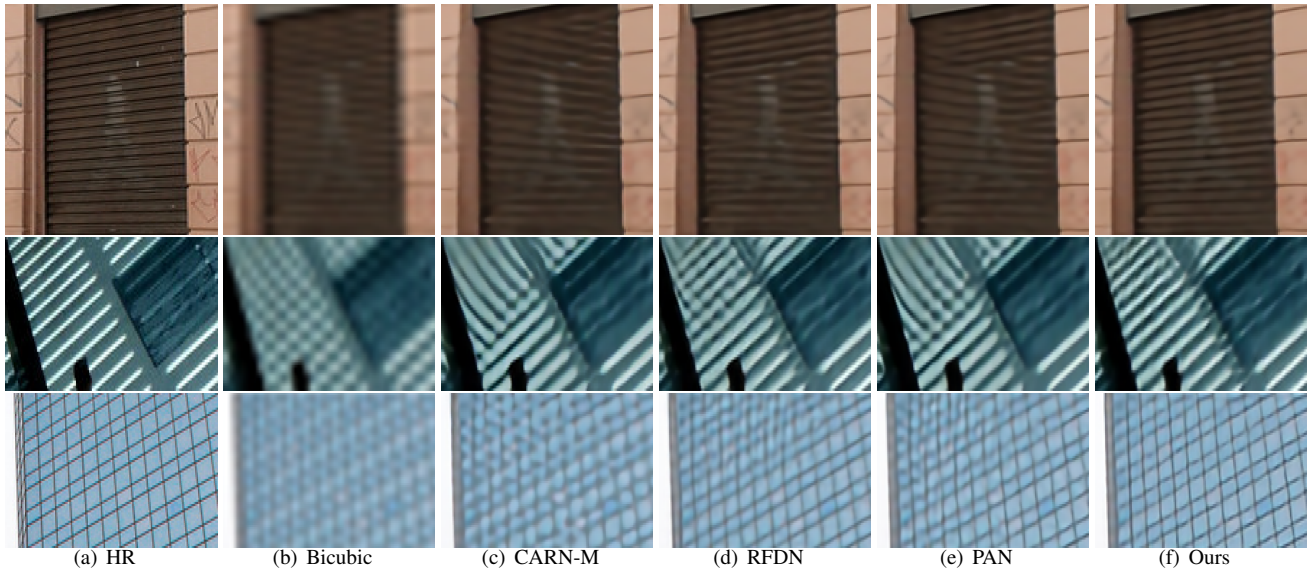


Figure 9. Visual comparisons among SOTA lightweight models in $\times 4$ image super-resolution. The test image patches are from Urban100. Note that the results of RFDN are based on our test with the pre-trained model which is officially released by the authors. Our method shows better reconstruction performance and less deformation on image details.